China Ocean Eng., 2021, Vol. 35, No. 3, P. 465–474
DOI: https://doi.org/10.1007/s13344-021-0043-y, ISSN 0890-5487
http://www.chinaoceanengin.cn/ E-mail: coe@nhri.cn

Pore Pressure Accumulation of Anisotropically Consolidated Soft Clay Subjected to Complex Loads Under Different Stress Paths

WANG Yu-ke[a, b, c], WAN Yong-shuai[a, c], RUAN Hang[b], YU Xiang[a, d, *], SHAO Jing-gan[e], REN De-bo[f]

[a] College of Water Conservancy Engineering, Zhengzhou University, Zhengzhou 450001, China

[b] State Key Laboratory of Geomechanics and Geotechnical Engineering, Institute of Rock and Soil Mechanics, Chinese Academy of Sciences, Wuhan 430071, China

[c] Collaborative Innovation Center of Water Conservancy and Transportation Infrastructure Safety, Zhengzhou 450001, China

[d] State Key Laboratory of Coastal and Offshore Engineering, Dalian University of Technology, Dalian 116024, China

[e] Henan Jiaoyuan Engineering Technology Co., Ltd, Zhengzhou 450001, China

[f] Yellow River Yuanyang Bureau, Yellow River Conservancy Commission, Yuanyang 453500, China

Received February 22, 2020; revised March 8, 2021; accepted April 8, 2021

Abstract

Owing to different influence factors of foundation soil, the initial stress state of the soil under various working conditions is complex. To simulate this situation, in this paper, a series of tests on undisturbed soft clay under pure principal stress axis rotation were carried out by using the hollow cylinder apparatus (HCA). The influence of initial consolidation angle ζ (the angle between the vertical direction and direction of the applied load in consolidation) and intermediate principal stress coefficient b on pore water pressure accumulation of undisturbed soft clay were mainly studied. The test results show that, during pure principal stress axis rotation, the pore water pressure accumulation of the undisturbed soft clay fluctuates and increases with the rotation of the major principal stress; the values of major principal stress angles α, corresponding to the peak value of the pore water pressure in a certain cycle, are different with different initial consolidation angles; the pore water pressure accumulation of soft clay is greatly affected by the intermediate principal stress coefficient b. With the fixed initial consolidation angle ζ, the variation trend of the maximum pore water pressure for each cycle is appropriately the same with different b values. With the increase of cycles, the difference value of pore water pressure between $b = 0$ and $b = 1$ in each cycle increases gradually with different initial consolidation angles ζ. While with different initial consolidation angles ζ, the increase of the pore water pressure when b increases from 0 to 0.5 is different with that when b increases from 0.5 to 1; the variation of maximum pore water pressure with ζ is significantly affected by the value of b; the value of maximum pore water pressure increases with the cycle number increases under all test conditions, but the growth rate decreases gradually. And the variation of maximum pore water pressure with the cycle number N is obviously influenced by both ζ and b.

Key words: anisotropical consolidation, pure principal stress rotation, soft clay, pore water pressure

Citation: Wang, Y. K., Wan, Y. S., Ruan, H., Yu, X., Shao, J. G., Ren, D. B., 2021. Pore pressure accumulation of anisotropically consolidated soft clay subjected to complex loads under different stress paths. China Ocean Eng., 35(3): 465–474, doi: https://doi.org/10.1007/s13344-021-0043-y

1 Introduction

With the sustained and rapid economic growth of China, a large number of infrastructures are being built, and various complex stresses in geotechnical engineering problems have become a factor which cannot be ignored in the current foundation disaster. However, cyclic loads such as traffic loads and so on will lead to complex responses, such as deformation characteristics, pore pressure generation and liquefaction resistance (Cui et al., 2014; Yang and Pan, 2017; Pan et al., 2019; Pan and Yang, 2020). A large area of

Foundation item: The work was financially supported by the National Key Research and Development Program of China (Grant No. 2019YFC1510803-2), the National Natural Science Foundation of China (Grant Nos. 51639002 and 51809034), the China Postdoctoral Science Foundation (Grant No. 2019M662533), the Open Research Fund of State Key Laboratory of Geomechanics and Geotechnical Engineering, Institute of Rock and Soil Mechanics, Chinese Academy of Sciences (Grant No. Z017012), and the Open Fund of State Key Laboratory of Coastal and Offshore Engineering, Dalian University of Technology (Grant No. LP2014).

*Corresponding author. E-mail: xiang_11_yu@yeah.net

saturated soft clay is distributed in the southeast coastal area of China, which is characterized by high water content, complex soil properties, low strength, high compressibility, poor permeability, strong structure and obvious anisotropy.

Most of infrastructures in coastal cities are built on soft soil foundation, the strain and pore water pressure accumulation caused by cyclic load can induce excessive deformation or instability of the structure foundation, which will affect the service life of the infrastructure, result in serious accidents, and even endanger the public interest and public safety. In practical engineering, the amplitude and direction of vertical stress and shear stress in the soil unit of infrastructure foundation change circularly, which results in complex and detrimental stress paths involving continuous principal stress axis rotation (Kirkgard and Lade, 1993; Qian et al., 2016; Wang et al., 2017a, 2018a, 2019), thus the strain development and pore pressure accumulation of the soil are caused. This kind of soil disturbance rather than the failure of the structure itself is the common reason for the structure damage. Owing to principal stress axis rotation, obvious pore water pressure accumulation is produced in soil mass (Towhata and Ishihara, 1985a), and even the liquefaction failure of soil mass can be led to. Pore water pressure is a basic consideration in engineering design, because the soil strength, deformation and other characteristics are directly affected by its development. Therefore, it is of great significance to study the pore water pressure of soft clay under continuous principal stress axis rotation, which can provide an important test basis for the construction and performance evaluation of civil engineering facilities in similar geological areas (Wu et al., 2020; Chen and Yang, 2017; Yang et al., 2019, 2020).

In recent decades, many experimental researches on pore pressure accumulation of sand, silt and clay under continuous principal stress rotation have been carried out by many researchers. Towhata and Ishihara (Ishihara and Towhata, 1983; Towhata and Ishihara, 1985a) analyzed the influence of shear stress level on pore water pressure characteristics of sand; Towhata and Ishihara (1985b) conducted cyclic shear tests on Toyoura sand under different stress paths involving principal stress rotation. The test results showed that there was a unique relationship between pore water pressure development and shear work; Symes et al. (1984). Sivathayalan and Vaid (2002) pointed out that the pore water pressure accumulation of sand would be restrained when the principal stress axial direction and the vertical axis direction were close. The test results of Symes et al. (1984), Nakata et al. (1998) and Chau and Zhao (2015) showed that the accumulation of pore water pressure and the plastic deformation can be induced only by the change of pure principal stress direction, thus the failure of sand occur. Yang et al. (2007) carried out experimental study on the undrained anisotropic behavior of saturated sand under the action of rotational shear, paying special attention to the effect of the intermediate principal stress coefficient on the pore pressure response. Stamatopoulos (2010) conducted monotonic and cyclic triaxial tests on sand mixtures containing 0%, 15% and 25% silt, the pore pressure accumulation in the soil, as well as the effects of sample density, consolidation stress and non-plastic fines on liquefaction strength was studied. From the perspective of energy through cyclic triaxial test, cyclic torsional shear test, different influences of cyclic stress ratio, frequency, relative density and cyclic stress path on pore water pressure development of silty soil were studied by Yan et al. (2011). It can be seen from the results that the collapse energy can be used as the cyclic strength standard of soil. And the relationship between pore pressure ratio and loss energy is related to frequency, density and stress path, but cyclic stress ratio is not taken into account. Wang et al. (2020a) studied the soft clay under the undrained cyclic principal stress rotation, thus, the effect of the consolidation ratio on the pore water pressure variation and the deviatoric strain was well understood under the action of vehicle load and wave load. To investigate the collapse characteristics of the high-density silt under the complex load, Yang et al. (2016) studied the high-density saturated silt at the estuary of the Yangtze River, and three groups of hollow cylinder tests were carried out to explore the influence of sample density, initial effective confining pressure and shear stress level on pore water pressure accumulation and liquefaction reaction of the samples. Lade and Kirkgard (2000) studied the effect of principal stress axis rotation and intermediate principal stress coefficient on pore water pressure accumulation of San Francisco Bay Mud. Qian et al. (2016) conducted a series of cyclic core-shaped and cyclic triaxial undrained tests on Shanghai clay using dynamic hollow cylinder apparatus (DHCA), during the test the torsional shear stress and normal stress were changed at the same time. Under the cyclic heart-shaped loading path and cyclic triaxial loading path, for different cyclic stress ratios, the pore pressure accumulation of the sample was studied by considering the principal stress axis rotation. Pan and Yang (2017) performed cyclic triaxial test to investigate the influence of initial shear stress and other factors on pore pressure generation characteristics of saturated sand under cyclic load.

Although relative researches on soft clay have been carried out by some researchers, most of the current experimental researches on pore pressure accumulation under continuous principal stress rotation are based on isotropic condition (Pan and Yang, 2017; Pan et al., 2018; Yang and Pan, 2018; Yang et al., 2018; Chen and Yang, 2020), it is necessary to conduct further researches on the response of anisotropic soft clay involved principal stress rotation. In this paper, the pore pressure accumulation of Wenzhou soft clay under different initial consolidation conditions is studied when the principal stress axis is rotating continuously at a large angle, and the influence of intermediate principal

stress coefficient is also considered.

2 Test materials and scheme

2.1 Test apparatus and test soil

The apparatus used in the test is GDS hollow cylinder torsional shear system, which can apply independently controlled axial force, torque and internal and external pressure on the hollow cylindrical specimen. Through the combined change of axial force, torque and internal and external pressure, the continuous principal stress axis rotation can be realized, and the magnitude of the three principal stresses as well as the major principal stress direction can be independently controlled. According to literature (Wang et al., 2017b, 2018b, 2019, 2020b), the introduction of the apparatus and calculation of stress and strain parameters of the sample are described in detail. The stress state and stress components of the hollow cylindrical specimen are shown in Fig. 1, besides, the stress path control parameters are shown in Eq. (1).

$$p=(\sigma_1+\sigma_2+\sigma_3)/3=(\sigma_z+\sigma_r+\sigma_\theta)/3; \tag{1}$$

$$q=(\sigma_1-\sigma_3)/2=\sqrt{(\sigma_z-\sigma_\theta)^2/4+\tau_{\theta z}^2}; \tag{2}$$

$$b=\frac{\sigma_2-\sigma_3}{\sigma_1-\sigma_3}=\frac{\frac{2\sigma_r-\sigma_z-\sigma_\theta}{2}+\sqrt{\left(\frac{\sigma_z-\sigma_\theta}{2}\right)^2+\tau_{\theta z}^2}}{\sqrt{(\sigma_z-\sigma_\theta)^2+4\tau_{\theta z}^2}}; \tag{3}$$

$$\alpha=\frac{1}{2}\tan^{-1}\left(\frac{2\tau_{\theta z}}{\sigma_z-\sigma_\theta}\right), \tag{4}$$

where p is the mean principal stress; q is the deviatoric stress; b is the intermediate principal stress coefficient; α is the angle between the major principal stress direction and the vertical direction; σ_1, σ_2 and σ_3 are the major, intermediate and minor principal stress, respectively; σ_θ, σ_r and σ_z are the circumferential, radial and axial stress, respectively; $\tau_{\theta z}$ is the torsional shear stress.

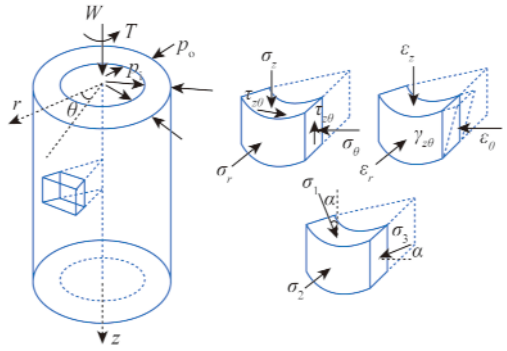

Fig. 1. Stress and strain states in hollow cylinder specimen.

The test soil is the natural clay sample taken from a foundation pit excavation site in Wenzhou. And the surface of the soil platform in the pit for taking samples is about 4 m below the ground surface. The water content of soil sample is 56%−59%, the soil specific gravity is 2.70, the initial density is 1.68−1.71 g/cm^3, the liquid limit is 64%, and the plasticity index is 36. In addition, the water saturation is 97%−100%, the initial void ratio is 1.51−1.55, and the water permeability is (6.60−6.84)×10^{-6} cm/s. The tested undisturbed soft clay block is prepared into a 200 mm×100 mm×60 mm (height×outer diameter×inner diameter) hollow cylindrical sample by special sample preparation equipment. The sampling of tested natural soil block and preparation method of hollow cylinder sample are given in the previous study (Wang et al., 2017b, 2018b, 2020b). The sample is saturated by back pressure, and when the saturation coefficient B-value reaches above 0.98, the sample is considered to be saturated. When consolidated, the major, intermediate and minor principal stresses are all 100 kPa. According to the consolidation process given by Zdravković and Jardine (2001), the isotropic consolidation is firstly carried out under the confining pressure of 50 kPa, and then the shear stress is gradually increased to the target value (10 kPa) with the mean effective stress remaining constant under the drainage condition, after that, the intermediate principal stress coefficient is adjusted to the target value through the operation interface. With keeping the added shear stress unchanged, the specimens are consolidated in different directions. When the drainage per hour is not more than 60 mm^3, the consolidation is considered to be completed.

2.2 Experimental scheme

The stress control method is adopted in the test. When the consolidation of the sample is completed, the principal stress axis is rotating purely under the undrained condition. The cyclic shear test is carried out for five cycles on the samples under different consolidation conditions and intermediate principal stress coefficients. The principal stress axial is rotating 180° in each cycle, and the cumulative rotation angle of α is defined as β in a single test. The shear rate of each test is 0.4°/min. In order to study the influence of the intermediate principal stress coefficient and initial consolidation angle on the pore pressure generation of undisturbed soft clay, a series of tests are designed. The specific test schemes are shown in Table 1.

3 Test results and analysis

3.1 Accumulation of pore water pressure with α under different ζ and b

In this paper, the ratio of pore pressure Δu to initial effective stress p' is defined as the pore pressure ratio. Figs. 2−6 show the relation curves between pore pressure ratio and major principal stress angle α under the condition of b = 0, 0.5 and 1 with different initial consolidation angles ζ. In Figs. 2−6, the variation curves of the pore pressure ratio from the first cycle to the fifth cycle (N=1, 2, 3, 4, 5) are respectively plotted by different line types.

Table 1 Test Schemes

Test ID	Initial consolidation angle ζ (°)	Confining pressure p (kPa)	Intermediate principal stress coefficient b	Deviatoric stress q (kPa)	(°)/N
A01			0		
A02	0		0.5		
A03			1		
B01			0		
B02	30		0.5		
B03			1		
C01			0		
C02	45	100	0.5	40	900 / 5
C03			1		
D01			0		
D02	60		0.5		
D03			1		
E01			0		
E02	90		0.5		
E03			1		

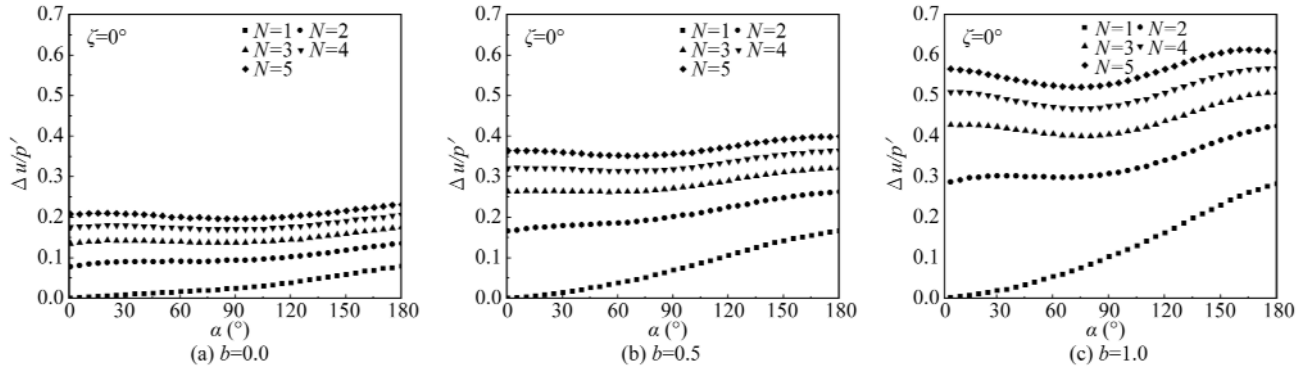

Fig. 2. Relationship curves between the pore pressure ratio and α with $\zeta = 0°$.

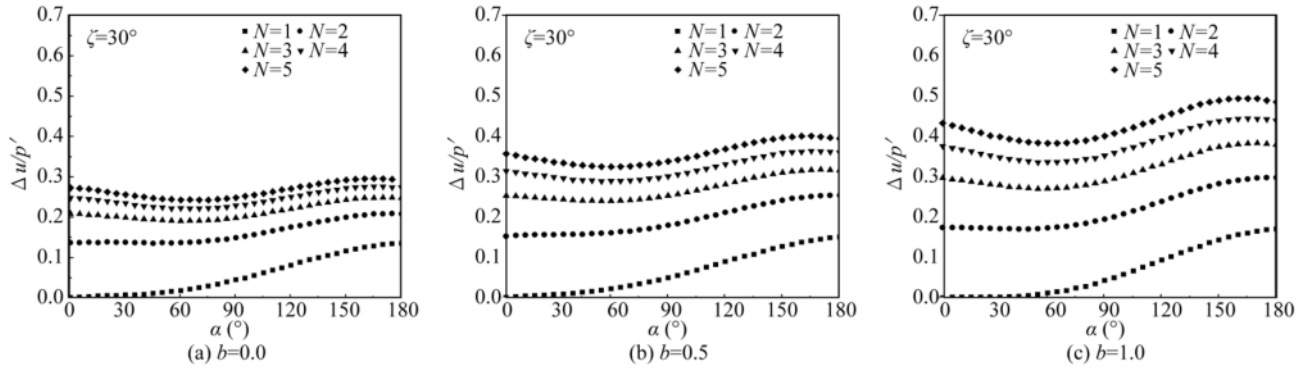

Fig. 3. Relationship curves between the pore pressure ratio and α with $\zeta = 30°$.

When ζ = 0°, the variation of pore pressure ratio for each cycle under different intermediate principal stress coefficients is shown in Fig. 2. When b = 0 and 1, the pore pressure ratio in the first two cycles increases gradually, while in the rest cycles, the pore pressure ratio first decreases and then increases; when b = 0.5, the pore pressure ratio in the first three cycles increases gradually, while in the rest cycles, the pore pressure ratio first decreases and then increases. However, it can be seen that the pore pressure of each cycle accumulates under various conditions. At the initial stage of the cycles, the pore pressure accumulates rapidly. With the increase of the rotation cycles, the accumulation of the pore pressure slows down. For example, when b = 0.5, the accumulated pore pressure ratio of the first cycle is 0.166, that of the second cycle to the fifth cycle are 0.097, 0.059, 0.043, 0.035, respectively. It is also not difficult to see from the figures that with the increase of b, the increasing rate of pore pressure ratio of the sample is increasing. It can also be seen that the increment of the pore pressure ratio when b increases from 0.5 to 1 is smaller than that when

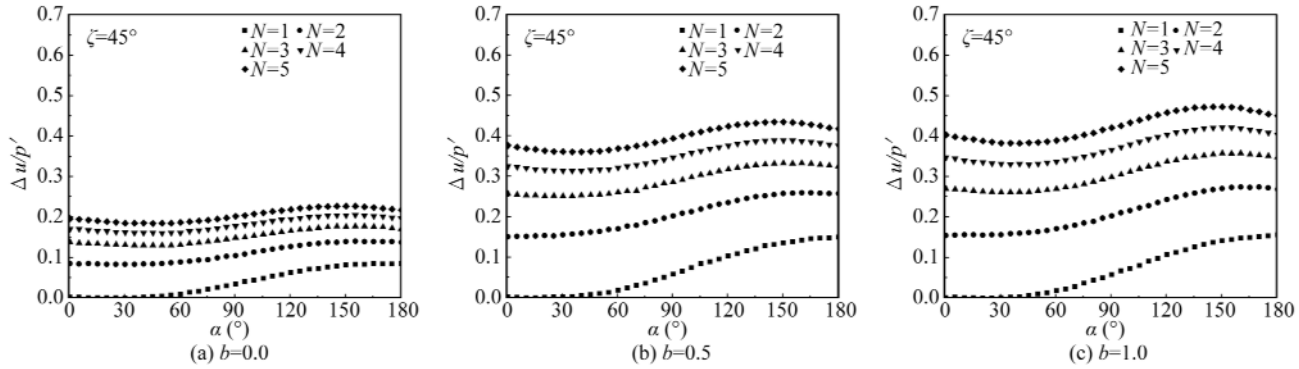

Fig. 4. Relationship curves between the pore pressure ratio and α with $\zeta = 45°$.

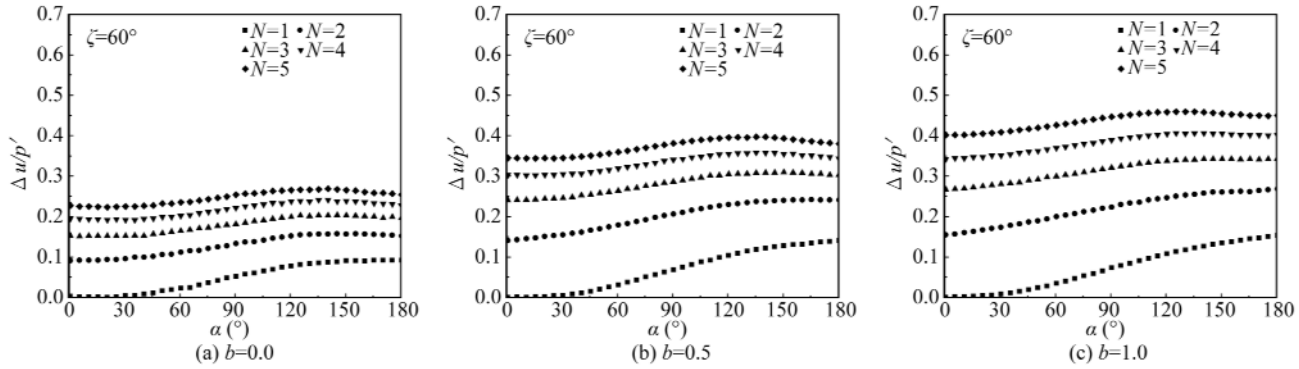

Fig. 5. Relationship curves between pore pressure ratio and α with $\zeta = 60°$.

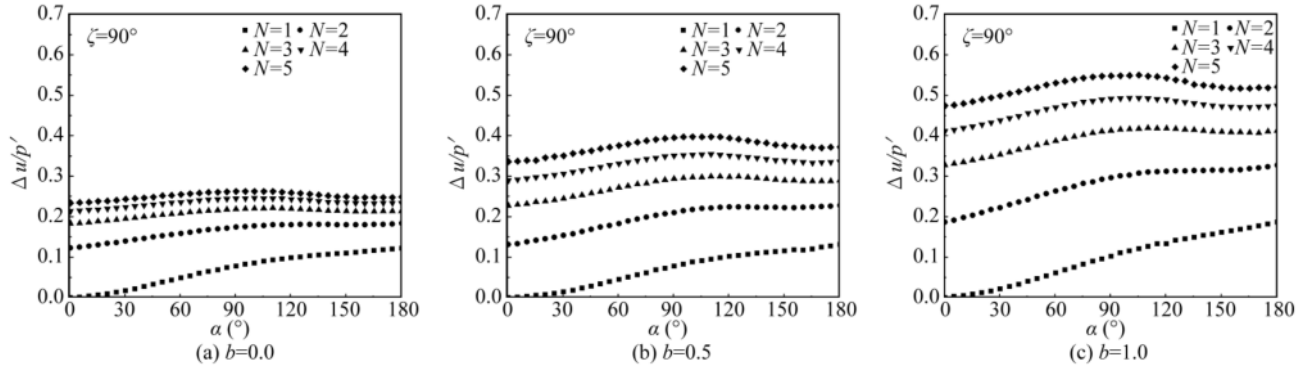

Fig. 6. Relationship curves between the pore pressure ratio and α with $\zeta = 90°$.

b increases from 0 to 0.5.

When ζ = 30°, the variation of pore pressure ratio for each cycle under different intermediate principal stress coefficients is shown in Fig. 3. When b = 0 and 1, the pore pressure ratio in the first cycle increases gradually, while in the other cycles, the pore pressure ratio first decreases and then increases, reaching the peak value and afterwards decreasing slightly; when b = 0.5, the pore pressure ratio in the first two cycles increases gradually, while in the other cycles, the pore pressure ratio first decreases and then increases, reaching the peak value and afterwards decreasing slightly. But it can be seen that, similar to ζ = 0°, the pore pressure of each cycle accumulates under various conditions. At the initial stage of the cycles, the pore pressure accumulates rapidly, and with the increase of the number of cycles, the accumulation of the pore pressure slows down. In addition, it can be seen that with the increase of b, the increasing rate of the pore pressure ratio becomes larger and larger. It can also be seen that the increment of the pore pressure ratio when b increases from 0.5 to 1 is smaller than that when b increases from 0 to 0.5.

When ζ = 45°, the variation of pore pressure ratio for each cycle under different intermediate principal stress coefficients is shown in Fig. 4. When b = 0 and 1, the pore pressure ratio in the first two cycles increases gradually, while in the rest cycles, the pore pressure ratio first decreases and then increases, reaching the peak value and afterwards decreasing to a certain extent; when b = 0.5, the pore pressure

ratio in the first three cycles increases gradually, while in the rest cycles, the pore pressure ratio first decreases and then increases, reaching the peak value and afterwards decreasing to a certain extent. It is not difficult to see that, compared with $\zeta = 0°$ and 30°, the α value corresponding to the valley value of the pore pressure ratio in this figure is reduced by about 30°. And similar to $\zeta = 0°$ and 30°, the pore pressure of each cycle accumulates under various conditions. At the initial stage of these cycles, the pore pressure accumulates rapidly, and with the increase of the number of cycles, the accumulation of the pore pressure slows down. In addition, it can be seen that with the increase of b, the increasing rate of the pore pressure ratio of the sample becomes larger and larger. It can also be seen that the increment of the pore pressure ratio when b increases from 0.5 to 1 is smaller than that when b increases from 0 to 0.5.

When $\zeta = 60°$, the variation of pore pressure ratio for each cycle under different intermediate principal stress coefficients is shown in Fig. 5. Under the condition of different b, the pore pressure ratio of the first two cycles increased gradually, while in the other cycles, different from $\zeta = 0°$, 30°, 45°, the pore pressure ratio increased firstly, and then decreased slightly after reaching the peak value. In the initial stage of the cycles, the accumulation of pore pressure ratio is relatively fast, and with the increase of the rotation cycles, the accumulation of pore pressure becomes slower. In addition, with the increase of b, the increasing rate of the pore pressure ratio of the sample becomes larger. From the figure, it is also not difficult to see that the increment of the pore pressure ratio when b increases from 0.5 to 1 is smaller than that when b increases from 0 to 0.5 in general.

When $\zeta = 90°$, the variation of pore pressure ratio for each cycle under different intermediate principal stress coefficients is shown in Fig. 6. Under the condition of different b values, the pore pressure ratio of the first two cycles increases gradually as a whole, while in other cycles, similar to $\zeta = 60°$, the pore pressure ratio increases gradually at first and then decreases to a certain extent after reaching the peak value. Compared with $\zeta = 60°$, the α value corresponding to the peak value of the pore pressure ratio in this figure is reduced by about 30°. Under each condition, the pore pressure of each cycle accumulates without exception. In the initial stage of the cycles, the pore pressure accumulates rapidly. With the number of cycles increasing, the pore pressure accumulation slows down. In addition, with the increase of b, the increasing rate of the pore pressure ratio of the sample becomes larger. It is also not difficult to see that the increment of the pore pressure ratio when b increases from 0.5 to 1 is larger than that when b increases from 0 to 0.5 in general.

It can be seen from Figs. 2−6 that during the pure principal stress axis rotation, under the condition that the mean effective principal stress and shear stress applied to the soft clay sample remain unchanged, the pore pressure ratio of the undisturbed soft clay increases with the increase of the major principal stress angle α, and fluctuates. In the first cycle, the increase of pore pressure ratio is the most significant, and the fluctuation is small, so it can be considered that the increase is approximately linear. Under different initial consolidation angles, the major principal stress angles corresponding to the peak value of the pore pressure ratio are also different in each cycle, which shows that the pore pressure accumulation is significantly affected by the stress path.

By comparing the accumulation curves of pore pressure ratio with the pure principal stress axis rotation under different consolidation angles, it can be seen that under the same consolidation angle, the effects of different intermediate principal stress coefficients b on the accumulation of pore pressure ratio are similar, with the increase of b, the accumulation value of pore pressure ratio increases. And under $\zeta = 30°$ and 45°, when $b = 0.5$ and $b = 1$, the pore pressure ratio is almost the same. The accumulation of pore pressure ratio at $\zeta = 45°$ is taken as an example, the pore pressure ratio accumulation value in the first two cycles is almost equal. At the end of the second cycle ($\beta = 2\times180°$), the pore pressure ratio corresponding to $b = 0.5$ and $b = 1$ is 0.255 and 0.270, respectively, while that corresponding to $b = 0$ is 0.138. At the end of the fifth cycle ($\beta = 5\times180°$), the pore pressure ratio corresponding to $b = 0.5$ and $b = 1$ is 0.418 and 0.452, respectively, while that corresponding to $b = 0$ is 0.217. At the end of rotation period ($\beta = 5\times180°$), when the initial consolidation angle $\zeta = 0°$, the pore pressure ratio is the largest (0.607) when $b = 1$, and it is the smallest (0.231) when $b = 0$. When the initial consolidation angle $\zeta = 30°$, the pore pressure ratio is the largest (0.422) when $b = 1$, and it is the smallest (0.293) when $b = 0$. When the initial consolidation angle $\zeta = 60°$, the pore pressure ratio is the largest (0.449) when $b = 1$, and it is the smallest (0.253) when $b = 0$. When the initial consolidation angle $\zeta = 90°$, the pore pressure ratio is the smallest (0.248) when $b = 0$, and it is the largest (0.519) when $b = 1$. And with the change of the initial consolidation angle, the major principal stress angle α corresponding to the peak value of the pore pressure ratio is also varying for each test, which is related to the peak value of the stress applied on the sample, and it is basically consistent with the conclusion of Kumruzzaman and Yin (2010).

When $b = 0$, 0.5 and 1, under pure principal stress axis rotation of undisturbed soft clay, the variation curves of pore pressure ratio with different initial consolidation angles are compared. Owing to the complex factors that affect the pore pressure accumulation, the development of pore pressure ratio varies under different conditions. When $b = 0$ and $b = 1$, the variation curves of the pore pressure ratio are more discrete than that of $b = 0.5$ under different initial consolidation angles, that is to say, when $b = 0$ and $b = 1$, the variation range of the pore pressure ratio is larger than that of $b = 0.5$ under each initial consolidation angle. At the end

of the rotation cycles (β = 5×180°), the difference of the pore pressure ratio is obvious between b = 0 and 1 under different initial consolidation angles. When b = 0.5, the pore pressure ratio of the sample is basically equal under different ζ. And when b = 1, the pore pressure ratio corresponding to ζ = 0° and ζ = 90° is larger than those of other conditions. At the end of the cycles, the pore pressure ratio of the sample is the largest when ζ = 0° and the smallest when ζ = 30°.

3.2 Accumulation of pore water pressure with b value under different ζ values

Fig. 7 shows the relationship between the maximum pore pressure Δu_m of different cycles and the intermediate principal stress coefficient b under various initial consolidation angles ζ. Obviously, the variation of Δu_m with b is similar at different initial consolidation angles, that is, with the increase of b from 0 to 1, Δu_m increases gradually, and the increased value for a single cycle of N=2−5 decreases. As the number of cycles increases, the value of Δu_m increases under the same b value, but the growth rate decreases. The pore pressure data at ζ = 45° is taken for analysis. When b = 0, Δu_m corresponding to N=1−5 is 8.4, 13.9, 17.7, 20.5, 22.7 kPa, and the increased value for a single cycle of N_2–N_5 is 5.5, 3.8 , 2.8, 2.2 kPa; when b = 0.5, Δu_m corresponding to N=1−5 is 15.0, 25.9, 33.3, 38.9, 43.4 kPa, respectively, and the increased value for a single cycle of N =2−5 is 10.9, 7.4, 5.6, 4.5 kPa; when b = 1, the corresponding Δu_m of N=1−5 is 15.5, 27.4, 35.9, 42.3, 47.3 kPa, and the increased value for a single cycle of N=2−5 is 11.9, 8.5, 6.4, 5.0 kPa. The data presented are in good agreement with the above conclusions.

It can also be seen from Fig. 7 that with the increase of rotation cycles, the difference Δu_c between b = 0 and 1 of each cycle gradually increases. The pore pressure data at ζ = 45° are also taken for analysis. Δu_c corresponding to N=1−5 is 7.1, 13.5, 18.1, 21.8, 24.6 kPa. From Fig. 7, it is not difficult to see that in a single cycle, when ζ = 0° and 90°, the increment of Δu_m when b increases from 0.5 to 1 is larger than that when b increases from 0 to 0.5. When ζ = 45° and 60°, it is opposite to that corresponding to ζ = 0° and 90°, that is to say, the increment of Δu_m when b increases from 0.5 to 1 is smaller than that when b increases from 0 to 0.5. When ζ = 30°, the increment of Δu_m when b increases from 0.5 to 1 is roughly equal to that when b increases from 0 to 0.5, that is, Δu_m increases linearly with the increase of b. In order to facilitate comparative analysis, the increment of Δu_m in the third cycle is defined as Δu_{z1} when b increases from 0 to 0.5 and Δu_{z2} when b increases from 0.5 to 1. When ζ = 0°, Δu_{z1} and Δu_{z2} are 14.7 kPa and 18.7 kPa respectively; when ζ = 30°, Δu_{z1} and Δu_{z2} are 6.7 kPa and 6.6 kPa respectively; when ζ = 45°, Δu_{z1} and Δu_{z2} are respectively 15.5 kPa and 2.6 kPa; when ζ = 60°, Δu_{z1} and Δu_{z2} are respectively 10.5 kPa and 3.3 kPa; when ζ = 90°, Δu_{z1} and Δu_{z2} are respectively 7.9 kPa and 12.0 kPa. The listed data can well support the above conclusion.

3.3 Accumulation of pore water pressure with ζ under different b

Fig. 8 shows the relationship between Δu_m of different

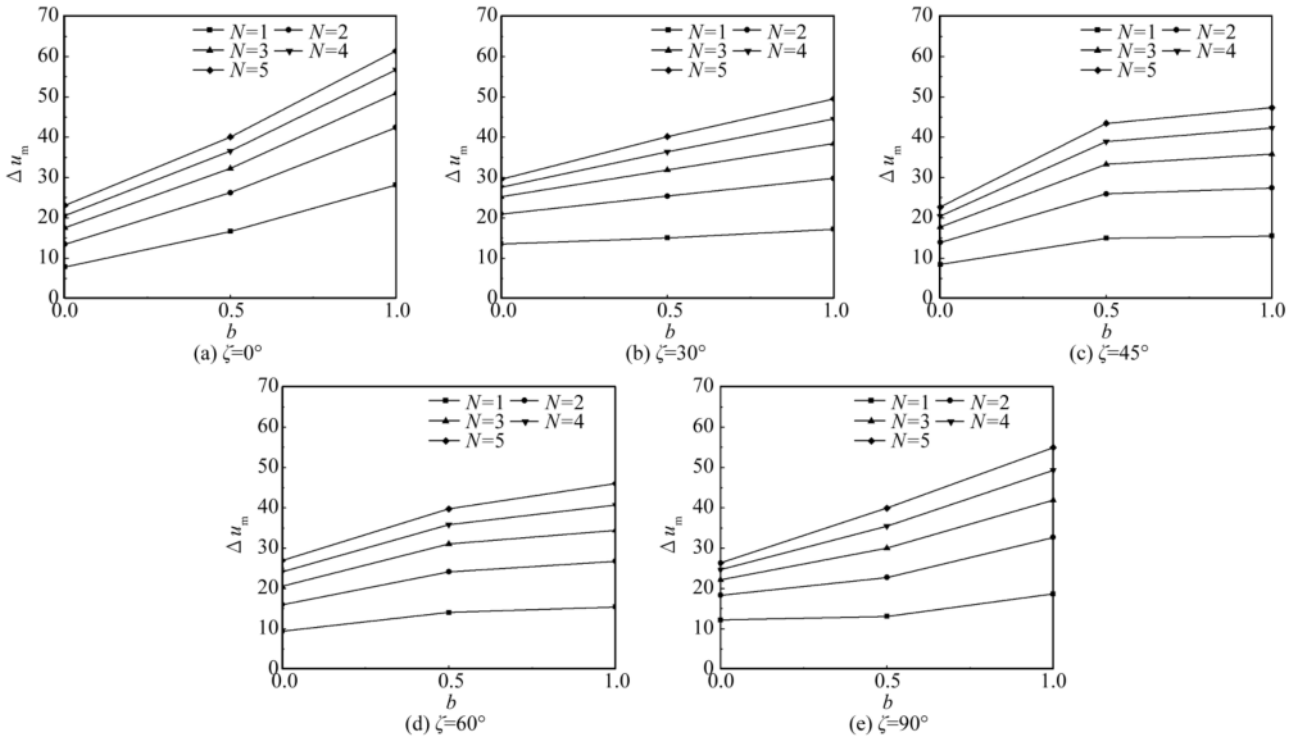

Fig. 7. Variation of pore water pressure with b at different ζ.

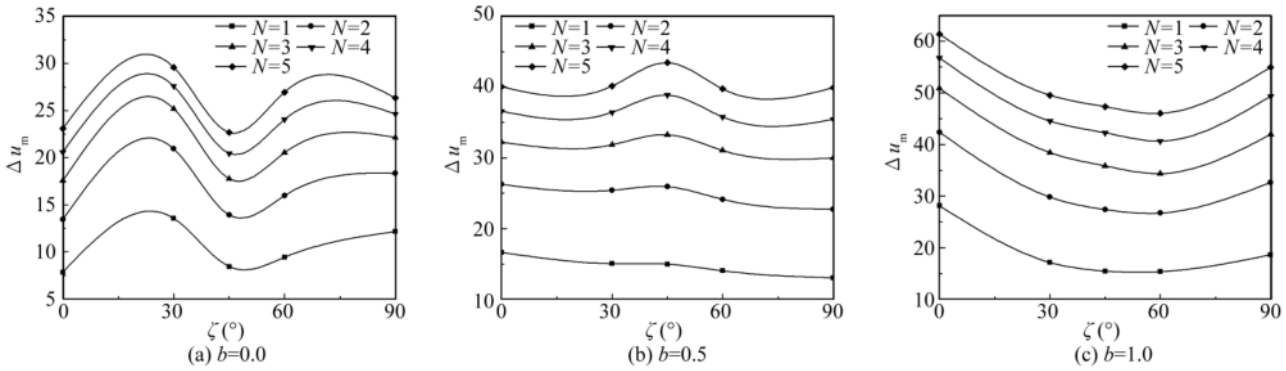

Fig. 8. Variation of pore water pressure with ζ under different b.

cycles and ζ under various b values. Obviously, the variation of Δu_m with ζ is significantly different under different b values. This may be due to the fact that the radial constraint of the intermediate principal stress on the sample is reflected by the value of the intermediate principal stress coefficient. If the radial constraint is too large or too small, the dispersion degree of pore pressure accumulation curve will increase.

When $b = 0$, with the increase of ζ, Δu_m firstly increases and reaches the peak value at about 22.5°, then decreases to the valley value at about 47.5° gradually. After the valley value, Δu_m always increases with ζ increasing to 90° when $N = 1-2$. While as $N = 3-5$, Δu_m first increases to the second peak value when ζ is between 70° and 75°, and subsequently decreases to some extent. And it can be easily seen that, the second peak value of Δu_m are all smaller than the first peak value of Δu_m. And it can also be seen that Δu_m increases when ζ increases from 0° to 90°. The increments are 4.34, 4.90, 4.58, 4.07 and 3.23 kPa corresponding to N=1−5; when $b = 0.5$, Δu_m decreases gradually with ζ increases from 0° to 90° for $N = 1$. For $N = 2$, with the increase of ζ, Δu_m firstly gradually decreases to the valley value at about 22.5°, then increases to the peak value at about 45° gradually. After the peak value, Δu_m always decreases with ζ increasing to 90°. For $N = 3-5$, with the increase of ζ, Δu_m firstly decreases and reaches the valley value at about 20°, then increases to the peak value at about 45°. After the peak value, Δu_m first decreases to the second valley value when ζ is between 70° and 80°, and subsequently increases to some extent. It can be easily seen that the second valley value is smaller than the first one for N =3, 4 and 5. The differences between Δu_m of $\zeta = 0°$ and 90° are 3.57, 3.51, 2.22, 1.17 and 0.12 kPa corresponding to N=1−5. It can be seen that the difference between Δu_m of $\zeta = 0°$ and 90° decreases gradually when N increases from 1 to 5; when $b = 1$, the variation of Δu_m is similar. With the increase of ζ, Δu_m decreases gradually to the valley value at about 60°, and subsequently increases gradually to some extent. But Δu_m for $\zeta = 90°$ is smaller than that for $\zeta = 0°$. The differences between Δu_m for $\zeta = 0°$ and 90° are 9.49, 9.73, 8.93, 7.39 and 6.41 kPa corresponding to $N = 1-5$. It can be seen that the difference between Δu_m for $\zeta = 0°$ and 90° decreases gradually when N increases from 1 to 5 in most cases. Besides, it is obvious that the fluctuation of Δu_m when $b = 0.5$ is smaller than those of $b = 0$ and 1. It due to that the radial constraint on the sample is reflected by the value of the intermediate principal stress coefficient. If the radial constraint is too large or too small, the fluctuation of pore water pressure will increase.

3.4 Accumulation of pore water pressure with N under different ζ and b

Figs. 9 and 10 show the variation of pore water pressure with N under different ζ and b values. It can be seen that the variation of Δu_m with N is similar under different ζ and b values, that is, Δu_m gradually increases with the increase of cycle number, but the growth rate decreases gradually. It indicates that the pore water pressure becomes stable gradually with the increase of the cycle number. From Fig. 9, it can be seen that Δu_m of $b = 1$ is always the largest, and Δu_m of $b = 0.5$ is always between those of b =0 and 1. It means that the accumulation for $b = 0.5$ is faster than that for $b = 0$, while smaller than that for $b = 1$. From Fig. 10, it can be seen that the variation curves of Δu_m with N for b =0.5 are almost coincident, which means that the influence of ζ on pore water pressure accumulation when $b = 0.5$ is not much. While the dispersion of variation curves for $b = 0$ and 1 are much higher. It means that the influence of ζ on the variation of Δu_m when $b = 0$ and 1 is much more obvious than that when $b = 0.5$. The reason is similar to that elaborated in the previous paragraph, that is, the pore water pressure is greatly influenced by the radial constraint which is reflected by b. If the radial constraint is too large or too small, the dispersion of variation curves for Δu_m will increase.

4 Conclusions

In this paper, through a series of tests under the stress path involving pure principal stress axis rotation, GDS hollow cylinder system (HCA) is used to study the effect of initial consolidation angle ζ and intermediate principal stress coefficient b on pore water pressure of Wenzhou soft clay.

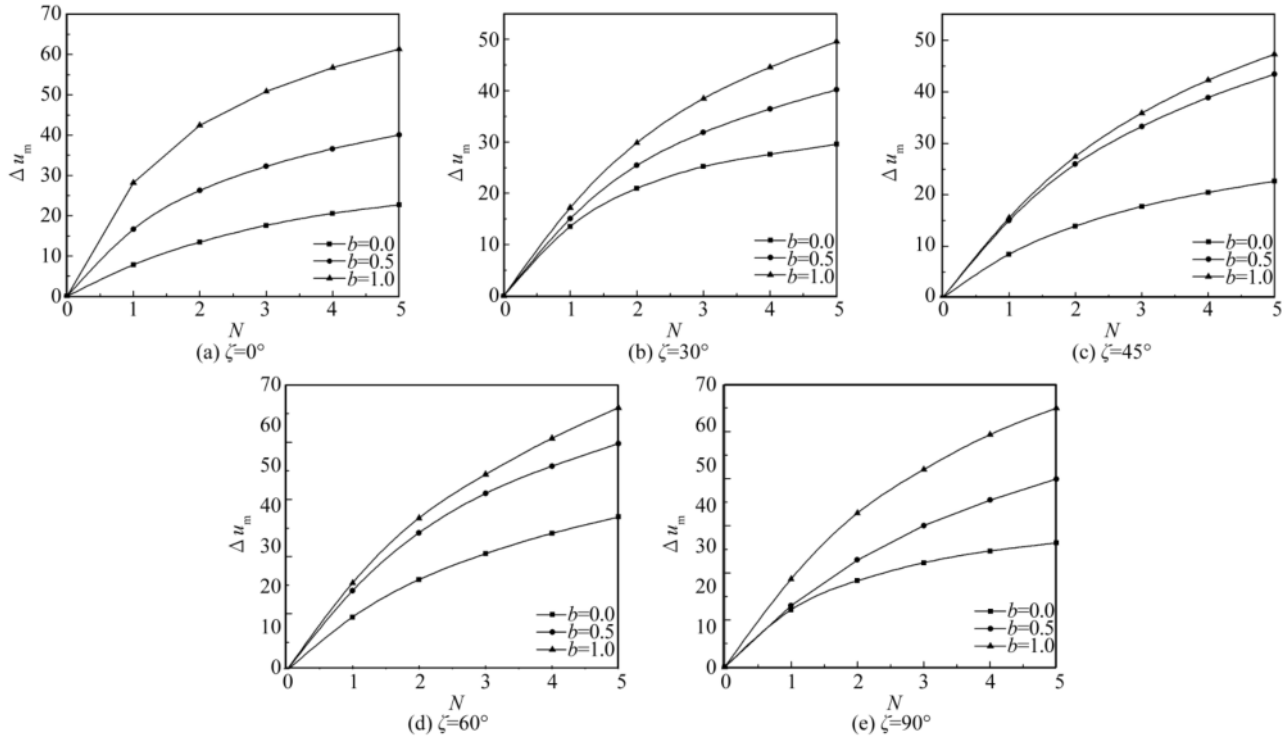

Fig. 9. Variation of pore water pressure with N under different ζ.

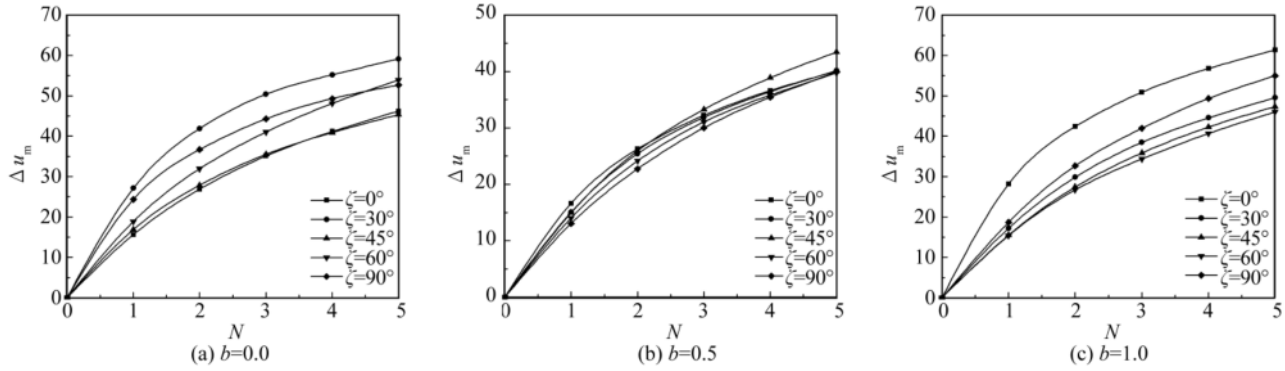

Fig. 10. Variation of pore water pressure with N under different b.

The main conclusions can be drawn.

(1) Under the condition of pure principal stress axis rotation, the pore pressure of the sample fluctuates and accumulates. For each test, in the initial stage, the pore pressure accumulates rapidly, and with the number of cycles increasing, the pore pressure accumulation slows down.

(2) The major principal stress angle α corresponding to the peak value of the pore pressure in a specific cycle decreases gradually with the initial consolidation angle increasing from 0° to 90°. At the same initial consolidation angle, the discreteness of the accumulation curves of the pore pressure ratio is influenced by the intermediate principal stress coefficient b to a certain degree. With the increase of b, the increasing rate of pore pressure is increasing, and the increment of the pore pressure ratio when b increases from 0.5 to 1 is different with that when b increases from 0 to 0.5 except for $\zeta = 30°$.

(3) At each initial consolidation angle, the variation of Δu_m with b is similar, that is, as b increases from 0 to 1, Δu_m increases gradually, and the increased value for a single cycle of N=2−5 decreases. In addition, with the number of cycles increasing, the difference Δu_c between b = 0 and b = 1 gradually increases in each cycle, while under different initial consolidation angles, the increase of Δu_m when b increases from 0 to 0.5 is different with that when b increases from 0.5 to 1 at most initial consolidation angles. In addition, the variation of Δu_m with ζ is significantly affected by b value.

(4) As the number of cycles increases, the value of Δu_m increases under different ζ and b values, but the growth rate decreases gradually. And the influence of both ζ and b on variation of Δu_m with N is obvious.

References

Chau, K.T. and Zhao, J.D., 2015. *Sand Degradation of Geomaterials in the New Millennium*, Springer International Publishing, Cham, 305–310.

Chen, Y.N. and Yang, Z.X., 2017. A family of improved yield surfaces and their application in modeling of isotropically over-consolidated clays, *Computers and Geotechnics*, 90, 133–143.

Chen, Y.N. and Yang, Z.X., 2020. A bounding surface model for anisotropically overconsolidated clay incorporating thermodynamics admissible rotational hardening rule, *International Journal for Numerical and Analytical Methods in Geomechanics*, 44(5), 668–690.

Cui, X.Z., Zhang, N., Zhang, J. and Gao, Z.J., 2014. In situ tests simulating traffic-load-induced settlement of alluvial silt subsoil, *Soil Dynamics and Earthquake Engineering*, 58, 10–20.

Ishihara, K. and Towhata, I., 1983. Sand response to cyclic rotation of principal stress directions as induced by wave loads, *Soils and Foundations*, 23(4), 11–26.

Kirkgard, M.M. and Lade, P.V., 1993. Anisotropic three-dimensional behavior of a normally consolidated clay, *Canadian Geotechnical Journal*, 30(5), 848–858.

Kumruzzaman, M. and Yin, J.H., 2010. Influences of principal stress direction and intermediate principal stress on the stress–strain–strength behaviour of completely decomposed granite, *Canadian Geotechnical Journal*, 47(2), 164–179.

Lade, P.V. and Kirkgard, M.M., 2000. Effects of stress rotation and changes of b-values on cross-anisotropic behavior of natural, K_0-consolidated soft clay, *Soils and Foundations*, 40(6), 93–105.

Nakata, Y., Hyodo, M., Murata, H. and Yasufuku, N., 1998. Flow deformation of sands subjected to principal stress rotation, *Soils and Foundations*, 38(2), 115–128.

Pan, K., Cai, Y.Q., Yang, Z.X. and Pan, X.D., 2019. Liquefaction of sand under monotonic and cyclic shear conditions: Impact of drained preloading history, *Soil Dynamics and Earthquake Engineering*, 126, 105775.

Pan, K. and Yang, Z.X., 2017. Effects of initial static shear on cyclic resistance and pore pressure generation of saturated sand, *Acta Geotechnica*, 13(2), 473–487.

Pan, K. and Yang, Z.X., 2020. Evaluation of the liquefaction potential of sand under random loading conditions: Equivalent approach versus energy-based method, *Journal of Earthquake Engineering*, 24(1), 59–83.

Pan, K., Yang, Z.X. and Xu, T.T., 2018. Impact of static preshearing on undrained anisotropy and shear characteristics of sand, *International Journal of Geomechanics*, 18(12), 04018162.

Qian, J.G., Wang, Y.G., Yin, Z.Y. and Huang, M.S., 2016. Experimental identification of plastic shakedown behavior of saturated clay subjected to traffic loading with principal stress rotation, *Engineering Geology*, 214, 29–42.

Sivathayalan, S. and Vaid, Y.P., 2002. Influence of generalized initial state and principal stress rotation on the undrained response of sands, *Canadian Geotechnical Journal*, 39(1), 63–76.

Stamatopoulos, C.A., 2010. An experimental study of the liquefaction strength of silty sands in terms of the state parameter, *Soil Dynamics and Earthquake Engineering*, 30(8), 662–678.

Symes, M.J.P.R., Gens, A. and Hight, D.W., 1984. Undrained anisotropy and principal stress rotation in saturated sand, *Geotechnique*, 34(1), 11–27.

Towhata, I. and Ishihara, K., 1985a. Undrained strength of sand undergoing cyclic rotation of principal stress axes, *Soils and Foundations*, 25(2), 135–147.

Towhata, I. and Ishihara, K., 1985b. Shear work and pore water pressure in undrained shear, *Soils and Foundations*, 25(3), 73–84.

Wang, Y.K., Gao, Y.F., Cai, Y.Q. and Guo, L., 2018b. Effect of initial state and intermediate principal stress on noncoaxiality of soft clay–involved cyclic principal stress rotation, *International Journal of Geomechanics*, 18(7), 04018081.

Wang, Y.K., Gao, Y.F., Guo, L., Cai, Y.Q., Li, B., Qiu, Y. and Mahfouz, A.H., 2017b. Cyclic response of natural soft marine clay under principal stress rotation as induced by wave loads, *Ocean Engineering*, 129, 191–202.

Wang, Y.K., Gao, Y.F., Guo, L. and Yang, Z.X., 2018a. Influence of intermediate principal stress and principal stress direction on drained behavior of natural soft clay, *International Journal of Geomechanics*, 18(1), 04017128.

Wang, Y.K., Gao, Y.F., Li, B., Guo, L., Cai, Y.Q. and Mahfouz, A.H., 2019. Influence of initial state and intermediate principal stress on undrained behavior of soft clay during pure principal stress rotation, *Acta Geotechnica*, 14(5), 1379–1401.

Wang, Y.K., Han, M.S., Yu, X., Wan, Y.S., Shao, J.G. and Ren, D.B., 2020b. Stiffness degradation of natural soft foundation in embankment dam under complex stress paths with considering different initial states, *Applied Ocean Research*, 104, 102356.

Wang, Y.K., Wan, Y.S., Liu, M.C., Guo, C.C., Zeng, C.N. and Wu, D., 2020a. Undrained multi-dimensional deformation behavior and degradation of natural soft marine clay from HCA experiments, *Soils and Foundations*, 60(1), 103–114.

Wang, Z., Yang, Y.M. and Yu, H.S., 2017a. Effects of principal stress rotation on the wave–seabed interactions, *Acta Geotechnica*, 12(1), 97–106.

Wu, Q.X., Xu, T.T. and Yang, Z.X., 2020. Diffuse instability of granular material under various drainage conditions: Discrete element simulation and constitutive modeling, *Acta Geotechnica*, 15(7), 1763–1778.

Yan, J., Shen, Y., Huang, G.F. and Yang, G., 2011. Energy-based method for analyzing the collapse characteristics of silt subjected to changes of principal stress orientation, *Journal of Testing and Evaluation*, 39(5), 760–765.

Yang, S., Wang X., Yan J. and Du W.H., 2016. Collapse characteristics of high-density silt under principal stress rotation, *Soil Mechanics and Foundation Engineering*, 53(2), 82–90.

Yang, Z.X., Li, X.S. and Yang, J., 2007. Undrained anisotropy and rotational shear in granular soil, *Géotechnique*, 57(4), 371–384.

Yang, Z.X., Liao, D. and Xu, T.T., 2020. A hypoplastic model for granular soils incorporating anisotropic critical state theory, *International Journal for Numerical and Analytical Methods in Geomechanics*, 44(6), 723–748.

Yang, Z.X. and Pan, K., 2017. Flow deformation and cyclic resistance of saturated loose sand considering initial static shear effect, *Soil Dynamics and Earthquake Engineering*, 92, 68–78.

Yang, Z.X. and Pan, K., 2018. Energy-based approach to quantify cyclic resistance and pore pressure generation in anisotropically consolidated sand, *Journal of Materials in Civil Engineering*, 30(9), 04018203.

Yang, Z.X., Xu, T.T. and Chen, Y.N., 2018. Unified modeling of the influence of consolidation conditions on monotonic soil response considering fabric evolution, *Journal of Engineering Mechanics*, 144(8), 04018073.

Yang, Z.X., Xu, T.T. and Li, X.S., 2019. J_2-deformation type model coupled with state dependent dilatancy, *Computers and Geotechnics*, 105, 129–141.

Zdravković, L. and Jardine, R.J., 2001. The effect on anisotropy of rotating the principal stress axes during consolidation, *Géotechnique*, 51(1), 69–83.